

Fluctuations in the Extragalactic Background Light: Analysis of the Hubble Deep Field¹

Michael S. Vogeley²

Princeton University Observatory

Princeton, NJ 08544-1001

vogeley@astro.princeton.edu

ABSTRACT

Statistical analysis of the unresolved light in the Hubble Deep Field (HDF) strongly constrains possible sources of the optical Extragalactic Background Light (EBL). This constraint is crucial for determining the spectrum of the EBL because reported upper limits on the optical EBL are several times larger than the surface brightness from detected galaxies, suggesting the possibility of additional galaxy populations. To test for the statistical signature of previously undetected sources, we estimate the auto, cross, and color correlations of the “sky” in the HDF that remains after masking objects brighter than $I_{814} = 30\text{mag}$. Auto and cross correlations of surface brightness in the V_{606} and I_{814} bandpasses are well-fitted by $\omega(\theta) \sim 10^{-6}(\theta/1'')^{-0.6}$ up to $10''$. Probable contributions of several instrumental systematics ensure that these correlations are firm upper limits on the true EBL fluctuations. This measurement yields the most stringent limits to date on small-scale structure in the night sky; analysis of shallower imaging would be dominated by galaxies now detected by the HDF.

Unless there is a truly uniform optical background, the mean EBL is likely to be within a small fraction of the surface brightness from detected galaxies. No currently plausible sources of additional EBL satisfy the constraints that they (1) would not have already been detected, (2) contribute EBL comparable to that from detected galaxies, and (3) do not produce EBL fluctuations in excess of the upper limits set by correlations in the HDF. These constraints admit only

¹ Based on observations with the NASA/ESA *Hubble Space Telescope*, obtained at the Space Telescope Science Institute, which is operated by AURA, under NASA contract NAS 5-26555

² Hubble Fellow

a confusion-limited population of extremely low surface brightness objects that is disjoint from the parameter space of all detected galaxies. Extrapolation of detected galaxy counts to zero flux would add only a few percent to the EBL. Diffuse intergalactic light clustered similarly to faint galaxies could explain some of the observed correlations but would contribute at most a few $\times 10\%$ to the mean EBL.

Subject headings: cosmology: observations – galaxies: clustering – galaxies: evolution – methods: statistical

1. INTRODUCTION

The Extragalactic Background Light (EBL) is the surface brightness of the night sky from all extragalactic sources, integrated out to the first epoch of star formation. The ultimate goal of studying the EBL is to complete the resolution of Olbers’s paradox by measuring the spectrum of the EBL, identifying the sources that contribute to it, and accounting for their evolution. Constraints on the optical EBL are particularly important because these bandpasses are sensitive to rest-frame UV flux from galaxies at $z > 1$, when we now believe the bulk of star formation in the universe occurred (Madau et al. 1996; Connolly et al. 1997). Thus, measurement of the spectrum of the optical EBL is a critical test for models of the star formation history of the universe (see, e.g., Whitrow & Yallop 1965; Partridge & Peebles 1967a,b; Fall, Charlot, & Pei 1996; Vaisanen 1996; Madau et al. 1997). Models for the sources of the EBL must also correctly predict statistical fluctuations in the EBL, which reflect the surface brightness profiles and clustering of these sources. [For an extensive review on the optical EBL that predates the HDF, see Tyson 1995.]

The average surface brightness of the sky from detected galaxies sets a firm lower limit on the mean EBL, $\bar{\mu}_{EBL} \geq \bar{\mu}_{galaxies}$ (here and throughout this paper, $\bar{\mu}$ is an average surface brightness). Tremendous progress has been made in detecting faint galaxies, through deep surveys such as the Hubble Deep Field (Williams et al. 1996) and the near-IR survey by Djorgovski et al. (1995), which reach as faint as $V = 29.5\text{mag}$ and $K = 24\text{mag}$, respectively. However, it is unclear what fraction of the mean optical EBL the detected galaxies comprise, because the uncertainties in the mean level of the optical EBL are larger than the surface brightness contributed by these galaxies. In addition, the systematic bias of object detection against relatively diffuse, low surface brightness objects leaves open the possibility that we may have missed a substantial fraction of the optical luminosity density in the universe (Disney 1976; McGaugh et al. 1995; Dalcanton 1997).

Figure 1 shows various observational constraints on the mean EBL. The inset box plots only the optical limits, using linear axes. Solid symbols indicate lower limits on the EBL in several bandpasses from the average sky brightness contributed by detected galaxies, $\bar{\mu}_{galaxies}$. In optical bandpasses, these lower limits include galaxy counts from the HDF and brighter counts from previous surveys (compilation by Pozzetti et al. 1997). UV galaxy counts are from Milliard et al. (1992). Open circles with 1σ uncertainties show a recent detection of the mean optical EBL (Bernstein 1997; Bernstein, Freedman, & Madore 1998). Arrows are upper limits from various experiments (Paresce 1990; Toller 1983; Dube, Wickes, & Wilkinson 1977, 1979; Hauser 1996), where the upper bound in each case is set primarily by uncertainties in foreground subtraction. Other bounds on the optical EBL (not plotted here) include experiments by Roach & Smith (1968), Lillie (1968), Spinrad & Stone (1978), Boughn & Kuhn (1986), and Mattila (1990). Precise measurement of the mean level of the EBL is extremely difficult because several foreground sources, particularly Zodiacal light, are at least an order of magnitude brighter than the mean optical EBL.

At optical wavelengths, uncertainties in the mean EBL leave room for considerable surface brightness above the lower limits set by galaxy detections. The 2σ uncertainties of the optical EBL detection by Bernstein et al. span the range from $\bar{\mu}_{EBL} \sim 0$ to $\bar{\mu}_{EBL} \sim 5\bar{\mu}_{galaxies}$. The gap between previous upper limits on the EBL and the galaxy surface brightness is of order 4 – 10. These uncertainties prompt us to examine the plausibility of an additional contribution to the EBL that is comparable to the surface brightness from detected galaxies with magnitude $V < 29.5\text{mag}$. Could this flux arise from fainter galaxies? The surface brightness per magnitude depends on the number counts as $dI_\nu/dm = (dN/dm)(I_{gal}(m)) \propto 10^{(\alpha-0.4)m}$. If we extrapolate the galaxy number counts to infinitely faint limits, assuming the logarithmic count slope $\alpha = 0.2$ at the HDF limit, then all galaxies with $V > 29.5\text{mag}$ would contribute only an additional 1.6% to the EBL. If, strangely, the number counts turn up to $\alpha = 0.3$ beyond $V = 29.5\text{mag}$, then this contribution rises to 3.3%. Thus, it seems unlikely that galaxies fainter than the HDF limit contribute significant flux. However, this does not rule out objects that evade direct detection, e.g., galaxies with total magnitude $V < 29.5$ and very low central surface brightness, or a diffuse intergalactic component.

If a substantial fraction of the EBL resides in sources that now lie below the detection limits of deep optical imaging, this population might be inferred from its statistical signature in the object-masked “sky.” The internal profiles of sources and clustering among them will cause correlations in the sky brightness. Differences between the spectra of these sources and the average sky brightness will yield corresponding fluctuations in color (for HST observations, the “average sky” is primarily Zodiacal light, for ground-based observations there is also a strong atmospheric component).

To constrain possible sources of additional EBL, we compute the angular autocorrelation function of the unresolved light in the Hubble Deep Field. In other words, we constrain additional sources of EBL by studying the correlation properties of the flux that cannot be assigned with large statistical significance to individual objects. Fluctuation analysis of the sky brightness is complementary to direct measurement of the mean EBL; although the uncertainties in direct measurement would permit a large EBL component in addition to detected galaxies, the small amplitude of the sky fluctuations rules out many plausible candidates for such a component. For example, we can statistically test the proposition that previously undetected low surface brightness galaxies comprise most of the EBL (Vaisanen 1996). This approach is insensitive to a truly uniform optical background, but the most plausible source of the EBL is emission from stars, which are likely to be clustered. At large redshift, we observe these in the rest-frame UV, where most of the stellar flux is from O and B stars. Regions of active star formation are extremely clumpy, so we expect the flux to be strongly correlated.

The approach of studying the correlation properties of the unresolved optical background was pioneered by Shectman (1974), who used Schmidt plates to detect optical EBL fluctuations on several arcminute scales. Shectman detected an EBL power spectrum that was consistent with clustering of galaxies fainter than $R = 18$, as predicted by Gunn (1965) and Shectman (1973). Tyson (1988) found evidence for residual surface brightness fluctuations in deep B band CCD images after cleaning detected $B < 27$ mag galaxies and smoothing on a scale of $6''$. Cole, Treyer, & Silk (1992) examined how fluctuation analysis of deep optical images might constrain faint galaxy populations. Martin & Bowyer (1989) detected arcminute-scale fluctuations with a rocket-borne UV detector, which indicated the presence of a UV background from galaxies. Boughn, Saulson, & Uson (1986) measured the beam-to-beam variance of the sky flux at $2.2\mu\text{m}$ to set upper limits on galaxy counts in the infrared, assuming a model for the galaxy clustering. Jenkins & Reid (1991) also measured sky fluctuations at $2.2\mu\text{m}$ to test galaxy evolution models. Recently, Kashlinsky et al. (1997) applied a fluctuation analysis to the DIRBE sky maps to set constraints on the infrared background. Fluctuations at zero lag have long been used to constrain the number count distribution of radio sources (Scheuer 1957; Hewish 1961; Condon 1974; see, e.g., Fomalont et al. 1988 for a recent result). Hasinger et al. (1993) computed limits on the X-ray flux distribution in deep ROSAT images and several analyses have been performed to measure the correlation function of the X-ray background, as observed by HEAO 1 (Persic et al. 1989) and Einstein (Barcons & Fabian 1989).

In this paper we use the Hubble Deep Field to probe the correlation structure of the night sky after masking all detected objects and thereby establish constraints on possible sources of the optical EBL. Section 2 presents estimates of the auto and cross correlation

of the unresolved sky in the Hubble Deep Field. Section 3 discusses possible contributions to these measurement from foregrounds and instrumental systematics. In Section 4 we use these results to set stringent limits on the types of additional galaxy populations that might lie hidden below current detection limits and examine if some of the measured correlation signal may be caused by weakly clustered intergalactic light. Section 5 reviews our conclusions.

We quote all HDF magnitudes in the AB system (Oke & Gunn 1983), defined as $AB = -2.5 \log f_\nu - 48.60$, where f_ν is in units of $\text{erg/s/cm}^2/\text{Hz}$. Distances are in $h^{-1}\text{Mpc}$, where the Hubble constant is $100h\text{km s}^{-1} \text{Mpc}^{-1}$.

2. EBL FLUCTUATIONS IN THE HUBBLE DEEP FIELD

2.1. Treatment of the HDF Data

We analyze the drizzled version 2 images of the HDF observed through the Wide Field cameras (WF) in the F450W, F606W, and F814W filters (hereafter we refer to these bandpasses as B_{450} , V_{606} , and I_{814} , respectively). Except for corrections to the flat field calibration (see below), we use the data as reduced and processed by the HDF team (Williams et al. 1996). We analyze only the central one-quarter of the area (roughly $41'' \times 41''$) of each drizzled image, to minimize the possible impact of residual large-scale gradients, and structure in the dark counts due to fluorescence of the MgF_2 window (Burrows et al. 1995). [For further details of the HDF, see <http://www.stsci.edu/ftp/science/hdf/hdf.html>.]

We apply corrections to the version 2 HDF images to remove large-scale gradients that are apparent after object-masking and smoothing of the remaining sky. Comparison of these features with ratio images formed from the v2 flat field calibrations and more recent calibration files (the latter are the calibration files currently used in the WFC2 pipeline) indicate that the gradients are caused by errors in the v2 calibrations. To remove these features we smooth the flat field ratio images (to remove small-scale noise) and multiply them into the HDF images. These gradients are quite small, typically 0.5% across an entire WF image, and are not expected to affect photometry of individual objects, because algorithms such as FOCAS estimate the sky level near each object. We remove these gradients because we are interested in detecting r.m.s. fluctuations in the sky at the level of 0.1%. In section we discuss the possible contribution of residual flat field uncertainty to the apparent sky fluctuations.

To prepare an object-masked image, we use the HDF version 2 FOCAS catalog to identify sources with total magnitudes brighter than $I_{814} = 30$ (Williams et al. estimate the

HDF to be 80% complete to $I_{814} = 29$), which includes virtually every object in the catalog. For comparison, we also derive catalogs from the HDF using the SExtractor package (Bertin & Arnouts 1996); we find the mask structure to be relatively insensitive to the choice of catalog and choose the available v2 FOCAS catalog to allow others to reproduce our results. The same mask, derived from detections in the summed $V_{606} + I_{814}$ image, is used for all filters. For each object we flag the pixels that lie within an ellipse that is twice as large as the area used by FOCAS to compute the “total magnitude.” The FOCAS “total magnitude area” is always at least twice the area within the detection isophote, so the masked area is at least four times as large as the isophotal detection region. Smoothing of the masked images on a range of scales does not reveal residual “doughnuts” around the masked objects. This masking procedure removes 30% of the pixels in each WF image. Therefore it does not appear that the sky is confusion-limited to the isophotal detection threshold of ~ 27 mag/arcsec² that was used for the FOCAS catalog.

2.2. Correlation Analysis

The field of view of the WF cameras is well-matched to probing EBL fluctuations caused by the correlation structure of galaxy profiles. The WF cameras each have a 80'' field of view of and 0.1'' pixel scale. At redshift $z = 1$, 1'' corresponds to 8.5kpc ($\Omega = 1$ and $H_0 = 50$ km/s). On these angular scales, the clustering amplitude of $I_{814} < 29$ galaxies is $\omega(1'') \lesssim 0.1$ (Colley et al. 1996; Villumsen et al. 1997). This weak clustering implies that small-scale fluctuations in the EBL will be dominated by the surface brightness profiles of faint objects rather than by the clustering among them.

For observed surface brightness $\mu(\mathbf{x})$, we define the autocorrelation function

$$C(\theta) = \langle \mu(\mathbf{x})\mu(\mathbf{x} + \theta) \rangle - \bar{\mu}^2, \quad (1)$$

where $\bar{\mu} = \langle \mu(\mathbf{x}) \rangle$. We often refer to the mean surface brightness $\bar{\mu}$ as the mean “sky” brightness (after masking detected objects, $\bar{\mu}$ corresponds to the usual definition of a “sky level”). We use Cartesian coordinates \mathbf{x} , with $\theta = |\mathbf{x} - \mathbf{x}'|$, because the relative angles in the HDF satisfy $\theta \ll 1$. The surface brightness autocorrelation may be written as the product of a dimensionless autocorrelation function and the square of the mean sky brightness

$$C(\theta) = \bar{\mu}^2 \omega(\theta). \quad (2)$$

To prepare an image for correlation analysis, we compute the mean value of the unmasked pixels and subtract this mean from the image, set pixels within the object ellipses to zero, and taper the edges of the image with a cosine bell function. To estimate the

autocorrelation function, we compute the Fourier transform of the image, square the moduli of the Fourier coefficients (for cross correlations, we compute the modulus of the products of the images’ Fourier coefficients) and correct these amplitudes for the effective area of the image after masking and weighting. We then inverse Fourier transform this two-dimensional power spectrum to produce the two-dimensional autocorrelation function. Averaging over all angles yields the function $C(\theta)$. Computation of $C(\theta)$ by direct summation of the products of the pixel values yields identical results (but uses significantly more CPU cycles). Analysis of test images with known power spectra confirm that we recover the true signal, after correcting for the integral constraint bias.

The integral constraint bias arises because we estimate the mean surface brightness $\bar{\mu}$ from the image itself. The implicit assumption that the ensemble average of μ is identical to the mean within the image is equivalent to assuming that there are no fluctuations of the mean surface brightness between different images. This bias causes us to underestimate the autocorrelation by the integral average of the true autocorrelation function over the area Ω of the image,

$$\Delta = \frac{1}{\Omega^2} \int d^2x \int d^2x' \omega_{true}(|\mathbf{x} - \mathbf{x}'|), \quad (3)$$

where ω_{true} is the true dimensionless autocorrelation function.

Figure 2 shows the dimensionless autocorrelation function of the object-masked HDF “sky” in each of the three bandpasses. In each case, we average the results for the WF2, 3, and 4 fields. Representative error bars are attached to the V_{606} curve only and are estimated from the variation among the three fields and within bins of width $\delta(\log_{10} \theta) = 0.4$. Near zero lag, the signal is dominated by photon shot noise over the scale of the $0.1''$ WF pixels. On scales from $0.15''$ to $8''$, these autocorrelation functions are well fitted by a power law

$$C(\theta) = \bar{\mu}^2 \omega(1'') (\theta/1'')^\gamma, \quad (4)$$

with $\gamma \sim -0.6$. Table 1 summarizes the power law fits and their uncertainties. At $1''$, the typical fluctuation is $\omega(1'') \sim 10^{-6}$, i.e., an r.m.s. correlated fluctuation of $\sim 0.1\%$ of the mean sky brightness, or ~ 30.5 mag/arcsec² in V_{606} .

The turnover of $\omega(\theta)$ on scales $\gtrsim 10''$ is consistent with the integral constraint bias that we expect for a power law correlation function over a field of this size. Using the power law fits in Table 1, we integrate equation (3) over a $41'' \times 41''$ field and find that the correlation functions in Figure 2 are underestimated by approximately $\Delta \sim 4 \times 10^{-7}$ (note heavy solid bar in Figure 2).

What could account for the power law shape of these correlations? In section 3 we discuss several instrumental systematics and foregrounds that might contribute to the

measured correlations. We note that the unmasked wings of the point spread function might cause correlations with similar shape to those plotted in Figure 2. To explain the shape of the correlation function with extragalactic sources, one can imagine an unclustered population of sources of different scale size such that the sum of their autocorrelations yields a power law. Alternatively, the similarity of the power law index, $\gamma \sim -0.6$, to that observed for galaxy clustering, $\gamma \sim -0.8$, suggests that the clustering of sources causes the power law shape. However, because we have reason to believe that systematics affect this measurement, it is premature to fit such models.

If we only mask galaxies brighter than $I = 26\text{mag}$, rather than $I < 30\text{mag}$, we find autocorrelations at $\theta < 0.5''$ that are an order of magnitude above the curves in Figure 2. This test indicates that fluctuation analysis of shallower imaging data would be dominated by the profiles of galaxies detected by the HDF. In ground-based imaging, this small-scale correlation structure would be smeared by seeing and the correlation signal from the profiles of galaxies in the magnitude range $26 < I_{814} < 29$ would be overwhelmingly larger than the signal measured in the HDF. In other words, the HDF is the first data set in which we could have detected a signal as weak as that shown in Figure 2. One might worry that, just as correlations in shallower imaging would be dominated by galaxies below the detection threshold, galaxies just fainter than the HDF limit dominate the observed correlations; in section 4 we show that this is not the case.

Cross correlations of images in different filters and comparison of these results with the respective autocorrelations provide a critical test of the nature of the observed fluctuations. Dot-dashed curves in Figure 2 show cross correlations of B_{450} vs. V_{606} and V_{606} vs. I_{814} . The cross correlations are shown as $\omega(\theta) = C_{1 \times 2}(\theta) / (\bar{\mu}_1 \bar{\mu}_2)$, where $\bar{\mu}_1$ and $\bar{\mu}_2$ are the mean sky levels. The photon count shot noise spike near zero lag is absent in the cross correlations because this source of noise is uncorrelated between the different images. Absence of this spike shows that the power law behavior of the correlations extends down to the smallest scale that we observe. This smallest scale is $0.04''$ rather than the $0.1''$ scale of the WF pixels, thanks to the sub-pixel resolution recovered by drizzling (see Fruchter & Hook 1997).

The close agreement between auto and cross correlations indicates that similar structure is present in different filters, in exposures that were obtained at different times. The relative amplitudes are consistent with a common origin for most of the fluctuations in all three filters, with some extra signal in the B_{450} and I_{814} images that is not present in V_{606} (V_{606} also has the highest signal-to-noise ratio). The dimensionless correlations in Figure 2 represent fluctuations relative to the mean sky level, thus the good match between correlations in different filters implies that the color of the fluctuating component must be close to that of the mean sky. It is important to remember that, because the mean sky is

much brighter than any possible EBL component, an instrumental systematic that varies slowly with wavelength could cause correlated structure with the same color as the mean sky.

We have also computed the autocorrelation function of the color of the unresolved sky, i.e., the ratio of surface brightness in different bandpasses (note that this is the ratio of measured surface brightness *before* subtracting the mean sky). Color correlations of the B_{450}/V_{606} and V_{606}/I_{814} ratio images, expressed as $\omega(\theta) = C_{1/2}(\theta)/(\bar{\mu}_1/\bar{\mu}_2)^2$, have slightly smaller amplitude and steeper slope than the auto and cross correlations. Color correlations should be relatively less affected by flatfield uncertainties because any wavelength-*independent* flatfield structure is divided out in forming the ratio image. We will report in detail on these results in Paper II (Vogele 1998). An important point is that we expect the amplitude of color correlations to be smaller than the individual filter autocorrelations by a factor that strongly depends on the relative color of the sources of the fluctuations and the mean sky. Here we note only that the detection of color correlation of the same order as the auto and cross correlations argues against a dominant systematic contribution from flatfield errors.

3. INSTRUMENTAL SYSTEMATICS AND FOREGROUND SOURCES

Several instrumental systematics and foreground sources may contribute to the clustering signal plotted in Figure 2. These effects include errors in calibration of the instrument sensitivity, smearing by the point spread function (PSF) of the telescope, wide-angle scattered light, and fluctuations in the Zodiacal and Galactic foregrounds. Because these systematics and foregrounds only add to the measured clustering signal, we may use the observed correlations as a firm upper limit on the true EBL fluctuations; this is the approach that we follow in Section 4 below. If we identify an instrumental effect that contributes to the fluctuations and subtract this contribution, then we obtain an even stronger constraint on additional sources of the EBL. For example, we have already been able to remove some signal by correction for obvious flatfield errors, and preliminary analysis clearly indicates a contribution from scattering by the telescope PSF. In Paper II we provide a detailed analysis of these possible contributions, with the goal of improving these upper limits.

3.1. HST/WFPC2 Systematics

Errors in calibration of spatial variations in the instrument sensitivity will cause apparent fluctuations in the sky. As noted above, smoothing of the object-masked sky revealed large-scale features in the v2 HDF images, which we removed using better flat field calibrations. Color correlation analysis removes signal caused by wavelength-independent flatfield errors, but this does not rule out a wavelength-dependent component. Another test is to compare the two-dimensional autocorrelation structure of the flatfields themselves with the detected signal. If the uncertainties in the flatfields are proportional to the flatfields themselves, then features in their two-dimensional autocorrelations will show up in the sky correlations. In addition to cross-correlating the flat field images with the data directly, we can compare the multipole moments of their two-dimensional autocorrelation functions. Preliminary analyses do not reveal cross correlations or anisotropies that are characteristic of flat field errors.

Measurement of the multipole moments can also reveal problems caused by charge transfer efficiency or other defects aligned with the CCD rows or columns, which cause a quadrupole signal. Scattered light from the HST secondary mirror support spider creates an “X” pattern that would yield a large hexadecapole moment.

The point spread function of the WFPC2 has extended wings, which probably arise from scattering inside the cameras (Krist & Burrows 1994; Krist 1995; Burrows et al. 1995). This PSF is anisotropic and varies with position within each camera. For our purpose, the most important effect of the PSF wings is to scatter some flux well beyond the mask region of an object. A crude test for this effect is to make an image in which we place a model of the PSF at the position of each detected object, with amplitude proportional to the measured magnitude, then mask this image as we do for the data and cross-correlate with the masked HDF image. Preliminary results from this and similar tests (such as varying the mask size) indicate that this effect produces correlations with shape that is similar to the HDF correlations and could contribute as much as 10 – 40% of the observed correlation amplitude. This may be the dominant systematic effect on our measurement. However, it is difficult to cleanly separate this PSF effect. Similar effects would arise if the profiles of detected galaxies extend far beyond the masked regions (i.e., if the sky is confusion-limited in these galaxies at some very faint isophote), or if lower surface brightness objects are clustered with the detected galaxies.

The dark count rate in the WFPC2 varies both spatially and temporally (Burrows et al. 1995). These variations are probably caused by fluorescence of the MgF₂ window on the camera. At fixed epoch, the dark count rate is constant within the central region of each field, but declines near the edges of the CCD. The amplitude of the dark count rate, and

therefore the steepness of the roll-off, varies in time with the cosmic ray flux. To minimize sensitivity to this effect, we restrict our analysis to the central one-quarter of the area of each CCD.

The drizzling procedure that was used to combine the HDF exposures includes corrections for the geometric field distortion in each camera. Restricting our analysis to the central area of each field also minimizes sensitivity to residuals from this distortion.

3.2. Foreground Sources

The motion of the Earth relative to the source of the Zodiacal light causes fluctuations in this foreground to be decorrelated between WFPC2 exposures. The Zodiacal light is Solar flux that is backscattered from a layer of dust that extends to roughly 3 A.U. (Dermott et al. 1996; Reach et al. 1996). In the time it takes for HST to orbit the Earth (96 minutes), the Earth’s motion around the Sun changes the HST’s line of sight through this dust layer. During the month of December (when the HDF was observed), the line of sight through a screen at a distance of 3 A.U. towards a fixed extrasolar target at $12^h37^m+62^\circ13'$ (the position of the HDF) changes by $\sim 2'$. The field of view of a WF camera is $\sim 1.25'$, therefore sky brightness fluctuations due to the Zodiacal foreground become decorrelated if we examine fluctuations by cross correlating WFPC2 exposures that are separated in time by at least the duration of one orbit. Exposures in different filters were separated by many orbits, thus cross correlations of images in different filters should be unaffected by ZL fluctuations. The good match of auto and cross correlations indicates that ZL fluctuations do not strongly affect any of our measurements.

The next brightest foreground is Galactic cirrus, which is presumably the reflection of starlight from high-latitude dust. The HDF field was chosen to lie at a minimum in the IRAS $100\mu\text{m}$ maps, thus we expect this Galactic foreground to be much smaller than average. Guhatakurta & Tyson (1989) measured the color of the Galactic cirrus and found that it is $\sim 1^m$ redder in $B_J - R$ than either the faint blue galaxies or the structure with surface brightness fainter than $\sim 30 \text{ mag/arcsec}^2$ seen on scales $> 6''$ by Tyson (1988). This color is similarly too red to match the color implied by the auto and cross correlations of the HDF sky (within a few tenths of a magnitude of the Zodiacal light color). However, because little is known about correlations of this foreground on scales of a few arcseconds, we cannot exclude this possibility.

4. CONSTRAINTS ON SOURCES OF THE EBL

4.1. Galaxy Populations

Is there a population of sources that (1) would not have been directly detected in the HDF, (2) would contribute significant surface brightness to the EBL, and (3) would not overproduce fluctuations in the EBL? If we specify the distribution of fluxes, surface brightness profiles, and angular clustering of a proposed undetected population, then we can compute the effect of these sources on fluctuations in the EBL. Using the measured correlations of the object-masked sky in the HDF as an upper limit on the true EBL fluctuations, we then test whether the predicted fluctuations are allowed by the measured sky correlations.

The autocorrelation of the surface brightness from a population of sources is the sum of contributions from the correlation structure within the profiles and from clustering among the sources. For a population of sources with identical apparent surface brightness profiles $\mu_{gal}(\theta)$, the autocorrelation function is

$$C_{galaxies}(\theta) = \bar{n}c_{gal}(\theta) + \bar{n}^2 \int d^2x c_{gal}(\theta - \mathbf{x})\omega_{clust}(\mathbf{x}). \quad (5)$$

The first term is from the correlations of flux within the object profiles; c_{gal} is the convolution of a galaxy profile with itself,

$$c_{gal}(\theta) = \int d^2x \mu_{gal}(\mathbf{x})\mu_{gal}(\mathbf{x} + \theta). \quad (6)$$

The second term is from clustering among the galaxies, with angular two-point correlation $\omega_{clust}(\theta)$.

In this subsection we assume that $\omega_{clust} = 0$, so that we can constrain possible EBL sources on the basis of their profiles alone. The addition of source clustering would increase the predicted EBL fluctuations and strengthen the constraints on these models. In the next subsection we examine the other extreme, a clustered diffuse EBL source.

Because it does not account for absorption of flux from one galaxy by dust in another, equation (5) is exact only in the limit where the sources are transparent or sparsely distributed. If galaxies have finite optical depth then we require more sources to produce fixed optical EBL. Another effect of absorption is that clustering of sources causes a smaller increase in the EBL fluctuations because nearby galaxies tend to shield one another. A complete accounting for these effects requires specification of the redshift distribution, spectral energy distribution, and extinction law for the sources. We will examine such detailed models in Paper III.

Here we consider only simple phenomenological source models, in which unclustered sources have exponential surface brightness profiles with identical apparent central surface brightness μ_0 and apparent angular scale length h . Such a population contributes total surface brightness

$$\bar{\mu}_{pop} = \bar{n}f = E\bar{\mu}_{detect}, \quad (7)$$

where \bar{n} is the projected number density, $f = 2\pi\mu_0h^2$ is the total flux of each source, and E is the ratio of this extra surface brightness to the surface brightness in detected galaxies to the HDF limit, $\bar{\mu}_{detect}$ (here we define $\bar{\mu}_{detect}$, which is the same as $\bar{\mu}_{galaxies}$ defined in section 1, to avoid confusion with the additional source population).

To compute the EBL fluctuations from this source population, we first compute the convolution of an exponential disk with itself,

$$c_{exp}(\theta) = c_{exp}(0)p(\theta/h) = \left(\frac{\pi}{2}\mu_0^2h^2\right) \left(\frac{2}{\pi} \int d^2u e^{-|u|} e^{-|u+\theta/h|}\right), \quad (8)$$

which defines a dimensionless profile function $p(\theta/h)$ with $p(0) = 1$. The autocorrelation of the population is

$$C_{pop}(\theta) = \bar{n}\frac{\pi}{2}\mu_0^2h^2p(\theta/h) = \frac{\bar{n}f^2}{8\pi h^2}p(\theta/h). \quad (9)$$

The power law fits to the HDF correlations (Table 1) yield a constraint on the EBL fluctuations caused by this population,

$$C_{pop}(\theta) < C_{obs}(1'')\theta^\gamma \quad (10)$$

for all θ . Combining the equations above, we derive a constraint on the the V_{606} band central surface brightness μ_0 and angular scale length h of these sources,

$$\mu_0 < 6.3 \times 10^{-22} (h/1'')^{-0.6} E^{-1} \text{ erg/s/cm}^2/\text{sr/Hz}. \quad (11)$$

If we define an effective area πh^2 for each source, then the covering factor (the average number of objects along a random line of sight) is of order

$$\chi = \bar{n}\pi h^2 = \frac{E\bar{\mu}_{detect}}{2\mu_0}. \quad (12)$$

Figure 3 shows the resulting constraints on the V_{606} band central surface brightness μ_0 and scale size h of a population of identical unclustered exponential disks that contributes mean surface brightness equal to that of detected galaxies ($E = 1$). The region below the solid line satisfies the constraint of equation (11). Above this line the sources'

autocorrelation function would exceed this upper limit for some range of θ . The right-hand axis indicates the covering factor χ for different μ_0 . Above the dashed line at the top of this figure lie objects directly detected in the HDF using FOCAS with an isophotal threshold of ~ 27 mag/arcsec². For a smaller contribution to the EBL, i.e., for $E < 1$, we relax the μ_0 limit by $2.5 \log E$ and change the covering factor by a factor E^{-1} . In the limit $E \lesssim 0.1$, the allowed region abuts the detected region.

Two examples of populations that contribute $\bar{\mu}_{pop} = \bar{\mu}_{detect}$ and marginally satisfy the correlation constraint illustrate how very different such a population would be from the HDF detections. For $h = 0.1''$ a population of extremely faint, total magnitude $V_{606} = 32.4$, sources with $\mu_0 = 29.4$ mag/arcsec² is marginally allowed. The number of such objects, $n = 1.3 \times 10^9 \text{deg}^{-2}$, is ~ 600 times the total number per deg² of detected galaxies. For $h = 1.0''$, the correlations allow a population of $V_{606} = 28.9$ mag sources, with $\mu_0 = 30.9$ mag/arcsec². For comparison, the typical scale size of $V_{606} = 29$ mag detected galaxies is $\lesssim 0.2''$. The projected number density of the additional $V_{606} = 28.9$ mag population would be 20 times the total number of detected objects. On the righthand axis of this plot we note the covering factor that corresponds to each choice of μ_0 and h . For the former example, this covering factor is $\chi \sim 3$, for the latter $\chi \sim 13$. Such large covering factors imply that these objects might be detected as QSO absorption line systems and/or from reddening of background objects.

For comparison to these models, note that the most extended low surface brightness galaxy seen to date, Malin 1, has an extrapolated disk central surface brightness of $\mu_0 = 26$ mag/arcsec² in V and scale size $h = 82h_{75}^{-1}$ kpc (Bothun et al. 1987). At $z = 0.5$ this would be dimmed to roughly 28 mag/arcsec² in I and would have an apparent scale size $h = 17''$. We obtain relatively poor constraints on sources with $h \gtrsim 10''$ because the integral constraint bias is comparable to the correlation function on these scales (see Table 1); the $41'' \times 41''$ field that we analyze is too small to accurately measure larger scale fluctuations. However, for $E = 1$, objects like Malin 1 clearly would be ruled out in Fig. 3 for a reasonable extrapolation of the measured correlation function.

Thus, to make a large contribution to the EBL, the correlation constraint requires that this additional population and the detected galaxies form an extremely bimodal distribution in surface brightness. The undetected sources must have very low central surface brightness and be confusion-limited on the sky. Some galaxies certainly lie within the region between the FOCAS detections and the “allowed” region for extra sources of the EBL. As shown in Section 1, extrapolation of the number counts would place some objects here but they would not contribute very much surface brightness to the EBL.

Extrapolation of the detected galaxy counts adds little to the EBL, but would these

fainter galaxies cause detectable correlations? No. Following equation (9), a population of galaxies fainter than m_{lim} with number per magnitude distribution $N(m) = d\bar{n}/dm$ and identical angular scale size h has zero-lag autocorrelation signal

$$C_{pop}(0) = \frac{1}{8\pi h^2} \int_{m_{lim}}^{\infty} dm N(m) \left[10^{-0.8(m+48.60)} \right] (\text{erg/s/cm}^2/\text{sr/Hz})^2. \quad (13)$$

If we extrapolate the HDF V-band counts from $V = 29.5\text{mag}$ to zero flux with logarithmic count slope $\alpha = 0.2$ and scale size $h = 0.2''$, then $C(0)_{pop} = 2.2 \times 10^{-43} (\text{erg/s/cm}^2/\text{sr/Hz})^2$, which translates to a dimensionless correlation $\omega_{pop}(0) = C_{pop}(0)/\bar{\mu}^2 = 2.2 \times 10^{-7}$. Comparison to Figure 2 shows that this signal is two orders of magnitude below the measured correlations. Thus, although galaxies brighter than the HDF detection limit would dominate the clustering signal (see section 2), galaxies just fainter than this limit have little effect on the observed correlations.

4.2. Weakly Clustered Diffuse Light

So far, we have ignored clustering among the undetected objects. If the undetected sources are clustered, then the solid line in Figure 3 moves down towards even lower allowed central surface brightness. In the limit of point-like objects, the autocorrelation function of a population (eq.[5]) reduces to

$$C_{pop}(\theta) = \bar{n} f^2 \delta(\theta) + \bar{n}^2 f^2 \omega_{clust}(\theta). \quad (14)$$

This must be convolved with the PSF to determine the observed autocorrelation. If we set $\bar{n} f = E \bar{\mu}_{detect}$ then we obtain a simple constraint on the $1''$ angular clustering amplitude of the sources,

$$\omega_{clust}(1'') < \frac{C_{obs}(1'')}{(E \bar{\mu}_{detect})^2}. \quad (15)$$

This constraint applies for all scales if we make the additional assumption that these objects have power law angular correlations, $\omega_{pop}(\theta) \propto \theta^\gamma$ with $\gamma \sim -0.6$, similar to that fit to the HDF sky correlations.

On scales larger than the PSF size, the inequality in equation (15) is equivalent to a constraint on a clustered diffuse EBL component with $\bar{\mu}_{diffuse} = E \bar{\mu}_{detect}$. Figure 4 shows the constraints on combinations of $\bar{\mu}_{diffuse}$ and $\omega_{diffuse}(1'')$ from the HDF correlations. For $E = 1$, the upper bound on angular clustering of diffuse light is $\omega_{diffuse}(1'') < 8 \times 10^{-3}$. This $1''$ clustering amplitude is an order of magnitude smaller than the clustering measured for galaxies as faint as $I < 29$ in the HDF (Colley et al. 1996; Villumsen et al. 1997). Thus, to contribute as much surface brightness as the detected galaxies, these undetected objects

must be not only extremely faint and numerous, but also uniformly distributed to exquisite precision.

Apart from *imagined* sources of additional EBL, several observations of galaxy clusters detect diffuse light or intergalactic stars that would contribute to the amplitude and clustering of the EBL if similar surface brightness is associated with most galaxies. From R band imaging of Abell 2029, Uson, Boughn, & Kuhn (1991) infer that 10% of the light in this cluster is in a diffuse component. Using WFPC2 imaging of the Virgo cluster, Ferguson, Tanvir, & Von Hippel (1996) find a population of intergalactic stars that could contribute total flux equal to 10% of that in galaxies. Theuns & Warren (1996) detect candidate planetary nebulae in Fornax and infer an intergalactic stellar population that contributes as much as 40% of the cluster light. Méndez et al. (1997) also find candidates for intergalactic planetary nebulae in Virgo. Tyson, Kochanski, & Dell’Antonio (1997) detect diffuse light in CL0024+1654 that comprises 15% of the light in the central 100kpc of this cluster.

If diffuse intergalactic light makes a fractional contribution to the EBL (relative to $\bar{\mu}_{detect}$ from galaxy counts) that is similar to the intergalactic surface brightness detected in clusters, then it could cause EBL fluctuations close to those measured in the HDF sky. The constraints on diffuse intergalactic light also follow from equation (15) if the diffuse light is clustered in similar fashion to faint galaxies, with a power law correlation function $C_{diff}(\theta) \sim \bar{\mu}_{diff}^2 \theta^{-0.6}$. Let us suppose that the clustering amplitude of the diffuse light is comparable to that of faint galaxies. The small arrow in Figure 4 indicates the level of diffuse light that contributes an additional $\bar{\mu}_{diffuse} = 0.1\bar{\mu}_{detect}$ (i.e., similar to the 10% contribution of intergalactic stars in Virgo). The EBL correlations from this source would match the HDF correlations if this light has the same clustering amplitude as $R < 23$ mag galaxies, $\omega(1'') \sim 1$ (Couch, Jurcevic, & Boyle 1993). Because 75% of the light from detected galaxies comes from $I_{814} < 23$ galaxies, it seems plausible that much of the diffuse light would be associated with galaxies in this same magnitude interval, and be gravitationally clustered with similar amplitude. Note that the contribution of any such a source to the EBL fluctuations would leave even less room in the upper limits on sky correlations for a discrete source population.

4.3. Is the HDF Typical?

A remaining question is whether the HDF is a typical field for the purpose of probing fluctuations in the EBL. The answer depends on the redshift and angular size of the hypothesized sources of undetected EBL. The $80'' \times 80''$ field of view of each WF camera limits the utility of the HDF for studying fluctuations on scales much larger than $10''$.

This angular coverage also limits the range of apparent magnitude of the galaxies that the field includes. Because this observation was designed to be an unbiased probe of the high-redshift universe, the field was deliberately chosen to avoid bright foreground galaxies ($V < 22\text{mag}$) which would fill much of the WFPC2 field of view.

This avoidance of bright galaxies raises the concern that the HDF is biased against detection of EBL fluctuations from previously undetected sources at redshift $z \lesssim 0.3$ that are clustered with bright galaxies. [A similar bias arises in the direct EBL detection method of Bernstein et al., because they use WFPC2 imaging to measure the total sky brightness.] However, it seems extremely contrived to envisage a population of sources that is not detected at $z > 0.3$ through fluctuation analysis, is not directly detected at $z < 0.3$ in deep ground-based imaging, and yet contributes a large fraction of the optical background.

Another issue is variation of EBL fluctuations from field to field. The total imaged area of the three WF cameras is 5.3 arcmin^2 , of which we analyze only the central 1.3 arcmin^2 . If additional sources of EBL are distributed similarly to the detected galaxies, then expected fluctuations in galaxy counts provides a rough estimate of uncertainty in the mean EBL over this area. The Poisson fluctuation in counts of galaxies with magnitude $26 < V < 29.5$ would be 5% over a 1.3 arcmin^2 area. For the magnitude range $23 < V < 26$, the expected fluctuation rises to 12%. Galaxy clustering does not significantly increase this lower bound on the field-to-field fluctuations; although the field of view spans only a few hundred kpc in angle, these magnitude intervals include galaxies over many hundreds of comoving Mpc in distance. We conclude that the field-to-field variation in the amplitude of the HDF correlations is likely to be caused by systematic effects rather than true fluctuations in the EBL.

5. CONCLUSIONS

Fluctuations in the object-masked sky in the HDF provide a strong, albeit indirect, constraint on the mean optical EBL. If the HDF provides a fair probe of the extragalactic sky between detected galaxies, then we conclude that this observation and other deep imaging surveys have already detected the sources of the majority of the optical EBL. The mean optical EBL is, at most, a few tens of percent above the mean surface brightness from detected galaxies. At $\lambda = 8100\text{\AA}$, a generous allowance for up to 50% additional EBL suggests $7.8 \times 10^{-6} \leq \nu I_\nu < 1.2 \times 10^{-5} \text{erg/s/cm}^2/\text{sr}$. This mean level lies at the lower end of the uncertainty range of the measurement by Bernstein et al. ($\nu I_\nu = 2.1 \pm 1.2 \times 10^{-5} \text{erg/s/cm}^2/\text{sr}$, after including $V < 23\text{mag}$ galaxies) and well below previous upper limits.

We infer this mean EBL level because no plausible sources of additional extragalactic surface brightness can satisfy the multiple constraints that these sources (1) have not already been detected, (2) contribute total surface brightness comparable to the surface brightness contributed by detected galaxies, and (3) do not produce EBL fluctuations larger than the upper limits set by correlations in the object-masked HDF. Figure 3 shows that these constraints admit only extremely low surface brightness objects that must be so extended and numerous as to be confusion-limited on the sky. The parameters of simple phenomenological models that meet these constraints would make such a population disjoint from the parameter space of all detected objects. Extrapolation of the HDF galaxy number counts to infinitely faint limits would add at most a few percent to the mean EBL. Figure 4 shows that a diffuse component that is as large as the surface brightness from detected galaxies would require a V -band angular clustering amplitude of $\omega(1'') < 8 \times 10^{-3}$, an order of magnitude less clustered than the faintest observed galaxies. Fluctuations in the EBL from intergalactic stars as seen in galaxy clusters could be as large as the upper limits on the fluctuations in the HDF, but would contribute only incrementally to the mean EBL.

In addition to constraining the plausible level of the optical EBL, these upper limits on small-scale sky fluctuations in the HDF provide a test for any proposed model for faint galaxy populations. We plan to test galaxy population models that are more detailed than the simple phenomenological model described in Section 4 (Paper III). We invite others to suggest possible models, compute the predicted autocorrelation function of sources below the detection limits, and compare with these limits from the HDF. These correlations are also important for attempts to detect weak lensing signals in deep optical imaging (Van Waerbeke et al. 1997; Refregier et al. 1997).

As we emphasize throughout this paper, the measured correlations of the object-masked sky in the HDF should be treated as upper limits on the true EBL fluctuations. The wings of the WFPC2 point spread function almost certainly contribute to the measured fluctuations. Although there are reasons to exclude flat fielding errors or Galactic light as the principal sources of the fluctuations, we cannot rule out some contribution from these effects. To improve these upper limits, we are examining these systematics and foregrounds in further detail (Paper II).

The HDF provides the best constraint to date on small-scale EBL fluctuations because its superior resolution allows detection of faint galaxy populations that would be confusion-limited in ground-based imaging. In section 2, we discuss how fluctuation analysis of shallower HST or ground-based images would be dominated on small scales by the profiles of galaxies that only the HDF detects. However, ground-based imaging is required to study fluctuations on angular scales much larger than several arcseconds, where access

to larger collecting area and accurate control of systematics outweigh the HST's advantages of high resolution and lower sky background. If we measure object-masked sky correlations in deep ground-based images, we can now use the HDF galaxy counts and profiles to model and subtract the surface brightness correlations that are caused by galaxies that are fainter than the ground-based detection limits, but that were detected by the HDF. Fluctuation analysis of deep ground-based imaging will allow statistical tests for diffuse intergalactic light on larger angular scales and for low surface brightness companions to galaxies that were too bright to be included in the HDF (see section 4c).

Future HST observations will allow measurement of EBL fluctuations in independent fields and at fainter surface brightness levels than the HDF. The planned HDF South (October 1998) will reach to similar depth and allow us to test if the HDF North is typical. The Advanced Camera for Surveys (scheduled for installation on HST in 1999) will have superior sensitivity and better-controlled systematic uncertainties than WFPC2, as well as a $200'' \times 200''$ contiguous field of view, thus allowing measurement of surface brightness fluctuations at fainter levels and somewhat larger scales. The proposed GTO program for ACS focuses on deep imaging of galaxy clusters. Fluctuation analysis of the ACS cluster fields will be an important test for sources of diffuse intergalactic surface brightness. In the $2 - 10\mu\text{m}$ infrared, the proposed Next Generation Space Telescope might detect statistical fluctuations in the EBL from the first generation of stars (e.g., Haiman & Loeb 1997) even if such objects evade direct detection.

We thank R. Williams and the entire HDF team, whose vision and effort made this project possible. We acknowledge discussions with and many helpful comments from A. Babul, R. Bernstein, S. Casertano, A. Connolly, H. Ferguson, A. Fruchter, M. Geller, E. Groth, R. Lupton, P. Madau, J. Peebles, A. Refregier, P. Stockman, M. Strauss, A. Szalay, T. Tyson, and D. Wilkinson. We also thank R. Bernstein and L. Pozzetti for providing results in advance of publication. This paper was initiated during a visit to the Aspen Center for Physics. Support for this work was provided by NASA through grants HF-01078.01-94A and AR-05812.01-94A from the Space Telescope Science Institute, which is operated by AURA, Inc. under NASA contract NAS5-26555,

REFERENCES

- Barcons, X., & Fabian, A. C. 1989, MNRAS, 237, 119
Bernstein, R. A. 1997, Ph.D. thesis, California Institute of Technology
Bernstein, R. A., Freedman, W. L., & Madore, B. F. 1998, in preparation

- Bertin, E., & Arnouts, S. 1996, *A&A Suppl.*, 117, 393
- Bothun, G. D., Impey, C. D., Malin, D. F., & Mould, J. R. 1987, *AJ*, 94, 23
- Boughn, S. P., & Kuhn, J. R. 1986, *ApJ*, 309, 33
- Boughn, S. P., Saulson, P. R., & Uson, J. M. 1986, *ApJ*, 301, 17
- Burrows, C. J., et al. 1995, *Wide Field and Planetary Camera 2 Instrument Handbook*, STScI publication
- Cole, S., Treyer, M., & Silk, J. 1992, *ApJ*, 385, 9
- Colley, W. N., Rhoads, J. E., Ostriker, J. P., & Spergel, D. N. 1996, *ApJ*, 43, 63
- Condon, J. J. 1974, *ApJ*, 188, 279
- Connolly, A. J., Szalay, A. S., Dickinson, M., Subbarao, M. U., & Brunner, R. J. 1997, *ApJ*, 486, L11
- Couch, W. J., Jurcevic, J. S., & Boyle, B. J. 1993, *MNRAS*, 260, 241
- Dalcanton, J. J. 1997, *ApJ*, in press
- Dermott, S. F., Jayaraman, S., Xu, Y. L., Grogan, K., & Gustafson, A. S. 1996, in *Unveiling the Cosmic Infrared Background*, ed. E. Dwek, *AIP Conf. Proc.* 348, 25
- Disney, M. J. 1976, *Nature*, 263, 573
- Djorgovski, S., Soifer, B. T., Pahre, M. A., Larkin, J. E., Smith, J. D., Neugebauer, G., Smail, I. Matthews, K., Hogg, D. W., Blandford, R. D., Cohen, J., Harrison, W., & Nelson, J. 1995, *ApJ*, 438, L13
- Dube, R. R., Wickes, W. C., & Wilkinson, D. T. 1977, *ApJ*, 215, L51
- Dube, R. R., Wickes, W. C., & Wilkinson, D. T. 1979, *ApJ*, 232, 333
- Fall, S. M., Charlot, S. & Pei, Y. C. 1996, *ApJ*, 464, L1
- Ferguson, H., Tanvir, N. & Von Hippel, T. 1996, *BAAS*, 189, 80.06
- Fomalont, E. B., Kellerman, K. I., Anderson, M. C., Weistrop, D., Wall, J. V., Windhorst, R. A., & Kristian, J. A. 1988, *AJ*, 96, 1187
- Fruchter, A. S., & Hook, R. N. 1997, in *Applications of Digital Image Processing XX*, ed. A. Tescher, *Proc. S.P.I.E.* vol 3164, in press (preprint astro-ph/9708242)
- Guhathakurta, P., & Tyson, J. A. 1989, *ApJ*, 346, 773
- Gunn, J. E. 1965, Ph.D. thesis, California Institute of Technology
- Haiman, Z., & Loeb, A. 1997, *ApJ*, 483, 21

- Hasinger, G., Burg, R., Giacconi, R., Hartner, G., Schmidt, M., Truemper, J., & Zamorani, G. 1993, *A&A*, 275, 1; erratum: 291, 348
- Hauser, M. G. 1996, in *Unveiling the Cosmic Infrared Background*, ed. E. Dwek, AIP Conf. Proc. 348, 11
- Hewish, A. 1961, *MNRAS*, 123, 167
- Kashlinsky, A., Mather, J. C., & Odenwald, S. 1997, *ApJ*, 473, L9
- Krist, J. E. 1995, in *Calibrating the Hubble Space Telescope: Post Servicing Mission*, eds. A. Koratkar & C. Leitherer, 311
- Krist, J. E., & Burrows, C. J. 1994, WFPC2 Instrument Science Report 94-01, STScI
- Lillie, C. F. 1968, Ph.D. thesis, University of Wisconsin
- Madau, P., Ferguson, H. C., Dickinson, M. E., Giavalisco, M., Steidel, C. C., & Fruchter, A. 1996, *MNRAS*, 283, 1388
- Madau, P., Pozzetti, L., & Dickinson, M. 1997, *ApJ*, submitted (preprint astro-ph/9708218)
- Martin, C., & Bowyer, S. 1989, *ApJ*, 338, 677
- Mattila, K. 1990, in *The Galactic and Extragalactic Background Radiation*, Proc. IAU Symp. 139, eds. S. Bowyer & C. Leinert (Dordrecht: Kluwer), 257
- McGaugh, S. S., Bothun, G. D., & Schombert, J. M. 1995, *AJ*, 110, 573
- Méndez, R. H., Guerrero, M. A., Freeman, K. C., Arnaboldi, M., Kudritzki, R. P., Hopp, U., Capaccioli, M., & Ford, H. 1997, *ApJ*, in press (preprint astro-ph/9710179)
- Milliard, B., Donas, J., Laget, M., Armand, C., & Vuillemin, A. 1992, *A&A*, 257, 24
- Oke, J. B., & Gunn, J. E. 1983, *ApJ*, 266, 713
- Paresce, F. 1990, in *The Galactic and Extragalactic Background Radiation*, Proc. IAU Symp. 139, eds. S. Bowyer & C. Leinert (Dordrecht: Kluwer), 307
- Partridge, B., & Peebles, P. J. E. 1967a, *ApJ*, 147, 868
- Partridge, B., & Peebles, P. J. E. 1967b, *ApJ*, 148, 377
- Persic, M., de Zotti, G., Boldt, E. A., Marshall, F. E., Danese, L., Francheschini, A., & Palumbo, G. G. C. 1989, *ApJ*, 336, L47
- Pozzetti, L., Madau, P., Zamorani, G., Ferguson, H. C., & Bruzual, G. A. 1997, *MNRAS*, submitted
- Reach, W. T., Franz, B. A., Kelsall, T., & Weiland, J. L. 1996, in *Unveiling the Cosmic Infrared Background*, ed. E. Dwek, AIP Conf. Proc. 348, 37
- Refregier, A., et al. 1997, in preparation

- Roach, F. E., & Smith, L. L. 1968, *Geophys. J.*, 15, 227
- Scheuer, P. A. G. 1957, *Proc. Camb. Phil. Soc.*, 53, 764
- Shectman, S. A. 1973, *ApJ*, 179, 681
- Shectman, S. A. 1974, *ApJ*, 188, 233
- Spinrad, H., & Stone, R. P. S. 1978, *ApJ*, 226, 609
- Toller, G. N. 1983, *ApJ*, 266, L79
- Theuns, T. & Warren, S. J. 1996, *MNRAS*, 284, 11
- Tyson, J. A. 1988, *AJ*, 96, 1
- Tyson, J. A. 1995, in *Extragalactic Background Radiation*, eds. D. Calzetti, M. Livio, & P. Madau (Cambridge University Press), 103
- Tyson, J. A., Kochanski, & Dell’Antonio, I. 1997, *ApJ*, submitted
- Uson, J. M., Boughn, S. P., & Kuhn, J. R. 1991, *ApJ*, 369, 46
- Van Waerbeke, L., Mellier, Y., Schneider, P., Fort, B., & Mathez, G. 1997, *A&A*, 317, 303
- Vaisanen, P. 1996, *A&A*, 315, 21
- Villumsen, J. V., Freudling, W., & da Costa, L. N. 1997, *ApJ*, 481, 578
- Vogeley, M. S. 1998, in preparation (Papers II, III)
- Whitrow, G. J., & Yallop, B. D. 1965, *MNRAS*, 130, 31
- Williams, R. E., Blacker, B., Dickinson, M., Dixon, W. V. D., Ferguson, H. C., Fruchter, A. S., Giavalisco, M., Gilliland, R. L., Heyer, I., Katsanis, R., Levay, Z., Lucas, R. A., McElroy, D. B., Petro, L., Postman, M., Adorf, H. M., & Hook, R. N. 1996, *AJ*, 112, 1335

Table 1: Autocorrelation and Cross Correlation Power Law Fits ^a

| Filter | $\omega(1'')$ | γ | $\bar{\mu}$ ^b | Δ ^c |
|--------------------------|----------------------------------|--------------------|--------------------------|-----------------------|
| B_{450} | $3.58 (\pm 0.69) \times 10^{-6}$ | $-0.80 (\pm 0.16)$ | 6.62×10^{-19} | 4.14×10^{-7} |
| V_{606} | $1.99 (\pm 0.38) \times 10^{-6}$ | $-0.61 (\pm 0.14)$ | 1.00×10^{-18} | 3.67×10^{-7} |
| I_{814} | $2.99 (\pm 0.59) \times 10^{-6}$ | $-0.59 (\pm 0.13)$ | 1.39×10^{-18} | 5.84×10^{-7} |
| $B_{450} \times V_{606}$ | $1.96 (\pm 0.39) \times 10^{-6}$ | $-0.62 (\pm 0.15)$ | ... | 3.53×10^{-7} |
| $V_{606} \times I_{814}$ | $2.14 (\pm 0.46) \times 10^{-6}$ | $-0.53 (\pm 0.14)$ | ... | 4.90×10^{-7} |

^aThe observed correlation function over $0.15'' < \theta < 8''$ is fit by $C(\theta) = \bar{\mu}^2 \omega(1'') (\theta/1'')^\gamma$.

^bMean of object-masked sky in $\text{erg/s/cm}^2/\text{sr/Hz}$. Note that $10^{-18} \text{ erg/s/cm}^2/\text{sr/Hz} = 22.94 \text{ AB mag/arcsec}^2$.

^cIntegral constraint bias for a $41'' \times 41''$ field, estimated using these fits (See eq.[3]).

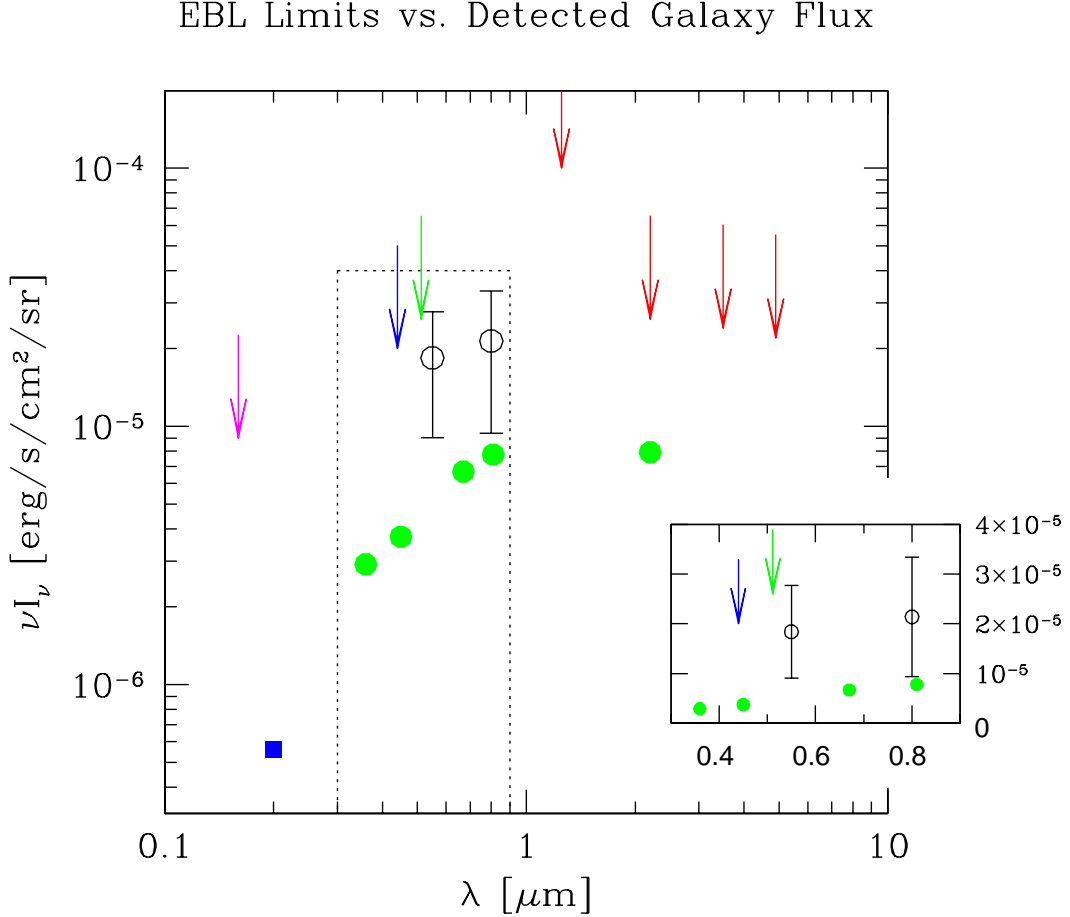


Fig. 1.— Observational constraints on the mean EBL. Inset box replots the dotted region (optical limits only) using linear axes. Solid symbols are lower limits from the average surface brightness contributed by galaxies detected in deep imaging surveys: the HDF, other optical surveys, and K-band (solid circles; Pozzetti et al. 1997), UV (square; Milliard et al. 1992). Arrows indicate upper limits on the extragalactic contribution to the night sky brightness in the UV from Paresce (1990), in the optical from Toller (1983) and Dube et al. (1977, 1979), and in the IR from Hauser (1996) (left to right, respectively). Open circles indicate a detection of the mean EBL (Bernstein 1997) with 1σ uncertainties. The detection level includes a small adjustment for flux from bright galaxies ($V < 23$ mag) that were excluded from this measurement. The surface brightness in AB magnitudes that corresponds to $\nu I_\nu = 10^{-5}$ erg/s/cm²/sr at $\lambda = 5500\text{\AA}$ is 27.3 mag/arcsec².

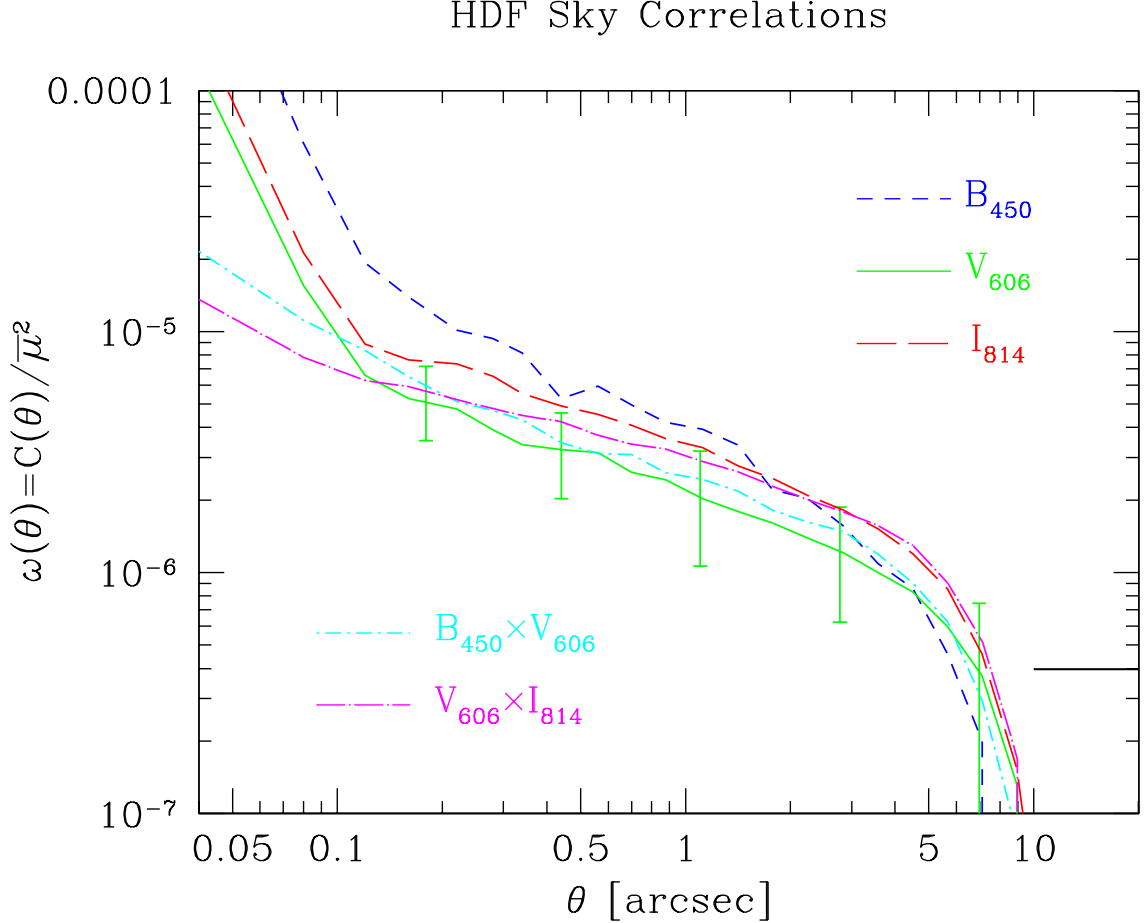


Fig. 2.— Autocorrelations of “sky” pixels in the central $41'' \times 41''$ of the HDF images in the B_{450} , V_{606} , and I_{814} bandpasses, and cross correlations of $B_{450} \times V_{606}$ and $V_{606} \times I_{814}$. These curves are averages over the WF2, 3, and 4 fields. Error bars on the V_{606} curve are from the variance among the fields (which dominates this uncertainty) and within bins of width $\delta(\log_{10} \theta) = 0.4$. Other curves have similar uncertainty. Shot noise dominates the autocorrelations for $\theta < 0.1''$. Both auto and cross correlations are well-fitted by power laws from $0.15''$ to $8''$ (see Table 1 for fitting parameters). The drop-off at large θ is an artifact of the integral constraint bias on the correlation function for a finite area of sky. The heavy solid bar at 4×10^{-7} marks the typical amount by which we underestimate the correlations due to this effect. Cross correlation removes the shot noise and confirms that roughly the same fluctuations are seen in different filters. Several sources of instrumental systematics and astronomical foregrounds may contribute to this measured correlation signal. Thus, we treat this measurement as an upper limit on small-scale fluctuations in the EBL.

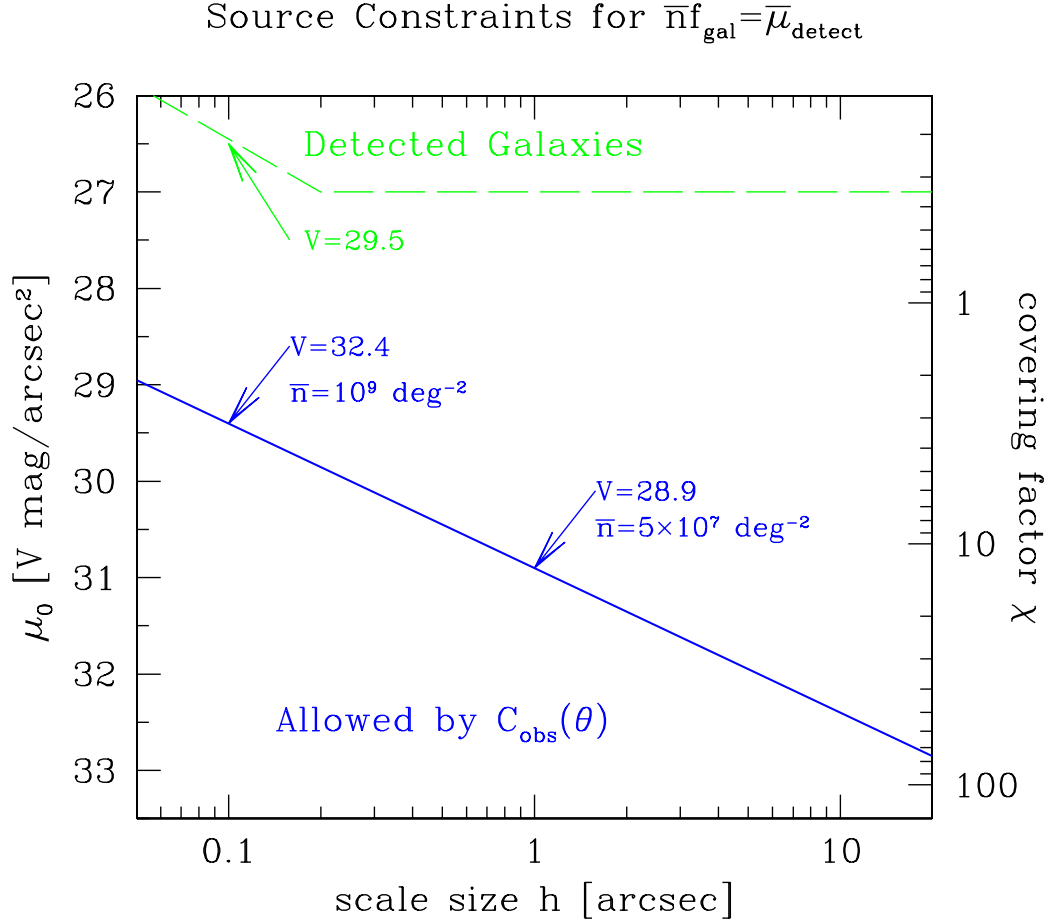


Fig. 3.— Correlation constraints on a population of identical exponential disks, assuming no clustering among the objects. Using the power-law correlation signal in Figure 2 as an upper limit on the true fluctuations, here we explore the allowed range of h and μ_0 in the V_{606} band. The surface density of objects is set so that the EBL contributed by these sources is equal to that in detected galaxies. A population with central surface brightness μ_0 and scale size h that lies above the solid line would produce correlations larger than observed. Below this line, the correlation constraint is satisfied, but the covering factor on the sky (right-hand axis) is quite large; any population with $\mu_0 > 29.5 \text{ mag/arcsec}^2$ would completely cover the sky > 3 times. Indicated are the total magnitudes and surface density of two marginally-allowed populations. The region above the dashed line is the locus of galaxies detected to the limits of the HDF. Some galaxies may exist between the dashed box and solid line without causing excessive EBL correlations; they simply cannot contribute very much total surface brightness to the EBL.

Constraints on Diffuse Light

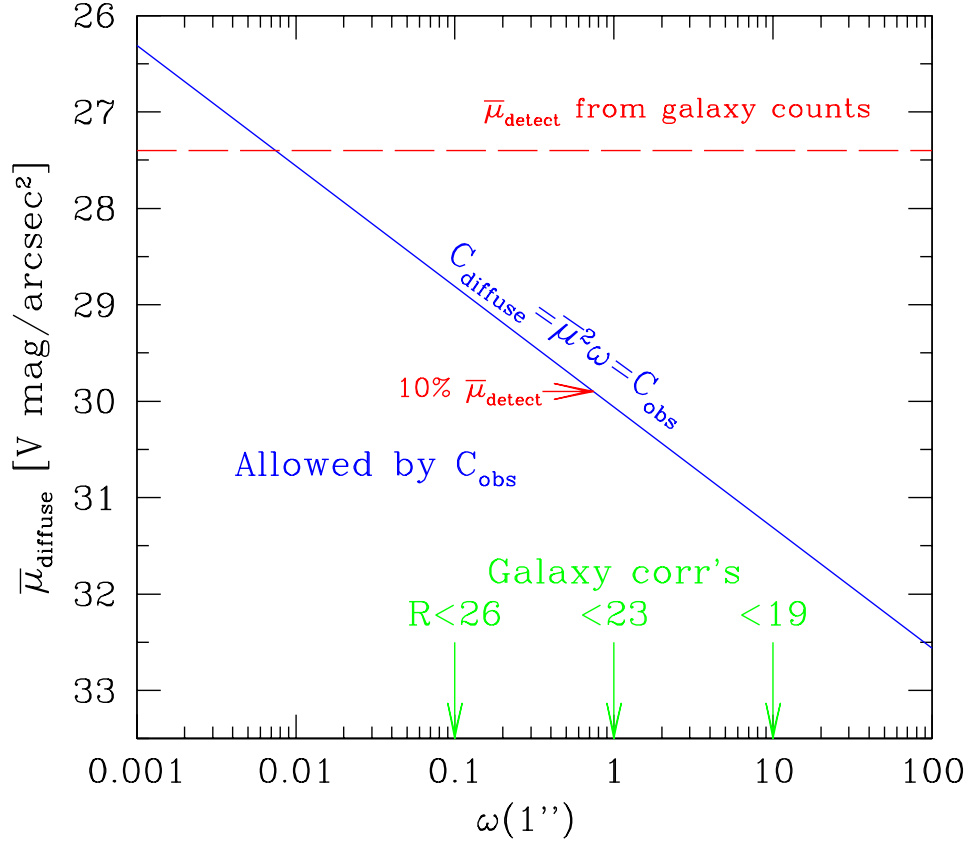


Fig. 4.— Constraints on clustered diffuse light with mean surface brightness $\bar{\mu}$ and $1''$ clustering amplitude $\omega(1'')$, assuming that the angular correlation function of the diffuse light has the same slope as the measured $\omega(\theta)$. The allowed region in the $\bar{\mu}-\omega(1'')$ plane lies below the solid line. To contribute surface brightness equal to that in detected galaxies (dashed line), the diffuse light would have to be nearly uniform. A small fractional contribution to the EBL, similar to the fraction of diffuse light in clusters, might be allowed if this light has angular clustering similar to faint galaxies (note arrows at bottom of this figure). The observed correlations marginally allow diffuse light with surface brightness that is $\sim 10\%$ that of detected galaxies if the correlation amplitude is similar to $R < 23\text{mag}$ galaxies. Note that 75% of the resolved EBL comes from galaxies with $I \lesssim 23\text{mag}$. Such an EBL component would account for the observed fluctuations but would add only incrementally to the total mean EBL.